Loss of Elongation-Like Factor 1 Spontaneously Induces Diverse, RNase H-Related Suppressor Mutations in *Schizosaccharomyces pombe*

Bahjat F. Marayati,[1] Alena L. Drayton,[1] James F. Tucker,[1] Reid H. Huckabee, Alicia M. Anderson, James B. Pease, Clifford W. Zeyl, and Ke Zhang[2]

Department of Biology, Center for Molecular Communication and Signaling, Wake Forest University, Winston-Salem, North Carolina 27101

ORCID ID: 0000-0003-1973-0874 (K.Z.)

ABSTRACT A healthy individual may carry a detrimental genetic trait that is masked by another genetic mutation. Such suppressive genetic interactions, in which a mutant allele either partially or completely restores the fitness defect of a particular mutant, tend to occur between genes that have a confined functional connection. Here we investigate a self-recovery phenotype in *Schizosaccharomyces pombe*, mediated by suppressive genetic interactions that can be amplified during cell culture. Cells without Elf1, an AAA+ family ATPase, have severe growth defects initially, but quickly recover growth rates near to those of wild-type strains by acquiring suppressor mutations. *elf1Δ* cells accumulate RNAs within the nucleus and display effects of genome instability such as sensitivity to DNA damage, increased incidence of lagging chromosomes, and mini-chromosome loss. Notably, the rate of phenotypic recovery was further enhanced in *elf1Δ* cells when RNase H activities were abolished and significantly reduced upon overexpression of RNase H1, suggesting that loss of Elf1-related genome instability can be resolved by RNase H activities, likely through eliminating the potentially mutagenic DNA–RNA hybrids caused by RNA nuclear accumulation. Using whole genome sequencing, we mapped a few consistent suppressors of *elf1Δ* including mutated Cue2, Rpl2702, and SPBPJ4664.02, suggesting previously unknown functional connections between Elf1 and these proteins. Our findings describe a mechanism by which cells bearing mutations that cause fitness defects and genome instability may accelerate the fitness recovery of their population through quickly acquiring suppressors. We propose that this mechanism may be universally applicable to all microorganisms in large-population cultures.

KEYWORDS elongation-like factor 1 (Elf1); suppressor; RNase H; genome stability; RNA nuclear accumulation

A healthy individual may carry severe, dominant, disease-associated mutations that are compensated by a second genomic perturbation (suppressor)—a phenomenon called genetic suppression (Harper *et al.* 2015). Suppressive interactions often occur between genes that have a close, functional connection. As a result, suppressor screens have been commonly employed to identify genes involved in a variety of biological pathways in bacteria, yeast, fly, and worm models (Manson 2000; Forsburg 2001; Jorgensen and Mango 2002; St Johnston 2002). Numerous studies indicate that naturally occurring genetic differences among individuals alter the phenotypic effects of mutations, leading to incomplete penetrance and variable expressivity among inbred laboratory model organisms (Dowell *et al.* 2010; Hou *et al.* 2015; Taylor *et al.* 2016). At present, it is not completely understood how distinct genetic lineages arise from a single parental species, or how single mutations affect the susceptibility to additional mutations.

Genomic stability during cell division is necessary to maintain the fidelity of haplotype transmission and reduce the rate of deleterious mutations. While mutations at low frequency contribute to genetic variation, a high frequency of genomic mutations (genome instability) is likely to severely impair cellular functions (Aguilera and García-Muse 2013). Despite

doi: https://doi.org/10.1534/genetics.118.301055
Manuscript received April 19, 2018; accepted for publication May 24, 2018; published Early Online May 29, 2018.
Available freely online through the author-supported open access option.
Supplemental material available at Figshare: https://doi.org/10.25386/genetics.6307136.
[1]These authors contributed equally to this work.
[2]Corresponding author: Department of Biology, Wake Forest University, Wake Downtown, 455 Vine St., Winston-Salem, NC 27101. E-mail: Zhangk@wfu.edu

multiple cellular mechanisms existing to preserve the genome and repair DNA damage (Ciccia and Elledge 2010), mutations inevitably occur, drive evolution and aging, and represent the basis of many genetic diseases, including cancer (Stratton *et al.* 2009; Pleasance *et al.* 2010).

External genotoxic stressors such as radiation, heavy metals, and chemicals can induce high levels of genome instability (Aguilera and García-Muse 2013). However, endogenous nuclear processes, such as transcription and replication, can also destabilize the genome (Gaillard *et al.* 2013; Costantino and Koshland 2015). Emerging views indicate that transcription induces hyper-mutation and recombination, potentially utilizing the intermediates or products made during transcription (Aguilera and García-Muse 2012; Skourti-Stathaki and Proudfoot 2014). RNAs can cause genome instability by reannealing to their template DNA strand forming DNA-RNA hybrids called "R-loops" (Sollier and Cimprich 2015). Without functional transcription elongation factors, R-loops can destabilize the genome by disrupting transcription and replication, resulting in replication stress and the formation of double-strand breaks (DSBs) (Aguilera and García-Muse 2012). DNA–RNA hybrids can also be produced by misincorporation of ribonucleotides into DNA during replication (Williams *et al.* 2016). Once formed, DNA–RNA hybrids are more stable than normal DNA strands, requiring extra energy to be resolved (Lesnik and Freier 1995).

Resolution of DNA–RNA hybrids, and alleviation of the subsequent mutagenic phenotypes, can be accomplished by overexpression of RNase H family proteins, which eliminate the RNA strands of DNA–RNA hybrids (Drolet *et al.* 1995; Gaillard *et al.* 2013). RNase H enzymes also remove RNA primers and misincorporated ribonucleotides during replication (Rydberg and Game 2002; Nick McElhinny *et al.* 2010). Failure to remove the incorporated ribonucleotides in DNA results in short deletion mutations and DNA-strand breaks (Williams *et al.* 2016). Considering the conserved, essential functions of RNase H enzymes, it is surprising that their activities are not required for survival in bacteria and lower eukaryotes, although they are indispensable for the development and survival of higher eukaryotes (Cerritelli and Crouch 2009).

In the fission yeast *Schizosaccharomyces pombe*, only nine proteins contain chromodomains. Eight of them have recognized chromatin-related functions such as binding to methylated histones and chromatin remodeling (Nakayama *et al.* 2000, 2001; Zhang *et al.* 2008; Shim *et al.* 2012; Touat-Todeschini *et al.* 2012; Al-Sady *et al.* 2013). However, the role of the ninth chromodomain protein, Elf1 (elongation-like factor 1), is not yet well-understood. Elf1 is in the ATP-binding cassette (ABC) class of the AAA+ protein family and has a reported role in RNA export (Kozak *et al.* 2002). We were initially prompted to study Elf1 based on our long-term interest in the function of chromodomain-containing proteins (Zhang *et al.* 2008). Although *S. pombe* cells lacking the chromodomain of Elf1 have no obvious growth defects compared to wild-type cells, we observed a severe growth defect following complete loss of Elf1. *elf1Δ* cells grow slowly, forming small colonies (P or parental strains), but can spontaneously convert to faster-growing strains (S or suppressed strains), which quickly outcompete P cells. Genetic analyses revealed that multiple, independent suppressor mutations caused the phenotypic recoveries of independently arisen S strains, implying that Elf1 has broad, epistatic functional interactions. Using whole genomic sequencing followed by genetic verification, we identified a few consistent suppressors of *elf1Δ*. A specific mutation in Cue2, an SMR (small MutS-related) domain-containing protein with implicated roles in mismatch repair, almost completely suppresses various cellular defects in *elf1Δ*. In addition to the self-recovery phenotype, we show that, without Elf1, cells are sensitive to DNA damage, have lagging chromosomes during cell division, easily lose nonessential mini-chromosomes, and abnormally accumulate RNAs within the nucleus. Notably, without RNase H activities, *elf1Δ* cells significantly increase the rate of phenotypic recovery, suggesting that nuclear RNA retention increases the formation of R-loops and/or the rate of ribonucleotide misincorporation into DNA, contributing to the rapid formation of suppressor mutations and quick phenotypic recovery in *elf1Δ*. Interestingly, cells without Mlo3 (an RNA export factor) or Rrp6 (the nuclear-specific exosome subunit), also accumulate RNAs within the nucleus but demonstrate distinct growth recovery patterns from that of *elf1Δ*, indicating that loss of Elf1, but not Mlo3 or Rrp6, can be almost fully compensated by secondary mutations, suggesting possible coevolution between Elf1 and its suppressors.

Materials and Methods

Strains and growth conditions

The *S. pombe* strains were generated using standard site-directed mutagenesis methods as previously described (Bähler *et al.* 1998), or by genetic crossing. The strains used in this study are listed in Supplemental Material, Table S1. All oligonucleotides used are listed in Table S2. Strains were grown in standard conditions on YEA rich media plates or liquid culture at 30° (Forsburg 2003). For preparing Edinburgh minimal media (EMM), EMM powder (catalog #:4110-012; Millipore Biochemicals) was filter-sterilized before added to preautoclaved agar. Thiamine Supplement was added at 12 μM (catalog #: BP892-100; Fisher BioReagents). To compare the size of colonies, cells were dissected using a microscope or manually spread, and typically grown on plates for 6 days so that colonies of *elf1Δ* P strains were of adequate size for imaging; all strains compared were grown for the same amount of time.

Strain type classification

To differentiate between *elf1Δ* strain-types that show different phenotypes, names were given based on the exhibited phenotypes. *elf1Δ* cells isolated from the meiotic cell cycle were designated "P" (parental). The P phenotype is defined by slow growth, abnormally long cells (Figure 1, A and B), and the formation of small colonies (average colony size,

0.849 ± 0.393 mm^2 after 6 days growth at 30°; Figure 1, B and F). *elf1Δ* cells that are not the fresh product of a meiotic cell cycle, but maintain the original slow growth phenotype were also called "P" cells. P-derived *elf1Δ* cells that spontaneously reverted (*i.e.*, without induced mutagenesis) to growth rates, cell shape, and colony size similar to wild type (8.13± 0.91 mm^2 after 6 days of growth at 30°) were designated as "S" (suppressed).

Strain type size analysis

To determine the size parameters for each type, P and S strains were streaked from −80° freezer stocks to isolate colonies on YEA plates. Both P and S strains were grown at 30°, and then cells from individual colonies were again isolated and spread on YEA plates by manual spreading or microscope dissection. These plates were grown at 30° for 6 days (±2 hr). The plates were equilibrated to room temperature, and then scanned at 600 dpi using an Epson Perfection V370 photo scanner. The sizes of each colony was measured using ImageJ software (version 1.47). The average colony sizes for all strains were calculated and checked for normality using a Shapiro-Wilk test (Figure 1). In Figure 3A, the colony size was measured after individual cells were dissected and grew on rich medium for 6 days. To ensure a clear distinction between P and S strain colonies, S strains were defined conservatively as those whose colony size was more than six times larger than the average size of P colonies. For genetic analysis shown in Figure 4 and Figure S2, even the colony size of a mutant is slightly smaller than that of the wild-type cells, as long as it is more than six times larger than the *elf1Δ* P cells, counted as wild-type colony size.

Survival competition assay

Wild-type cells, incapable of growing on media containing antibiotics (Nat$^-$, nourseothricin sensitive) were combined in liquid YEA with an equal amount of *elf1Δ* mutant cells (P or S) or wild-type control strains with an antibiotic-resistance gene (Nat$^+$, nourseothricin resistant). A small sample of this cell mixture was immediately spread onto YEA plates and incubated at 30° until distinct colonies were visible, then replica plated onto YEA plates containing antibiotics. Only cells containing antibiotic resistance genes were able to survive on these plates, which allowed for the calculation of the starting ratio of wild-type and mutant cells (Day 0). The rest of the cell mixture was placed in a shaking incubator and grown overnight. The next day, a sample of the liquid culture was transferred to a new tube of fresh liquid YEA to an optical density at 595 nm (OD_{595}) of 0.01. The fresh culture was allowed to grow overnight, and this process was repeated for 6 days of total growth in liquid YEA media. After 6 days of growth, a small sample was plated onto YEA plates. The plates were incubated at 30° until distinct colonies were visible, then replica plated onto YEA plates containing antibiotics. Only cells containing antibiotic resistance genes were able to survive on these plates, and the resulting number of colonies was used to calculate the final ratio of wild-type and

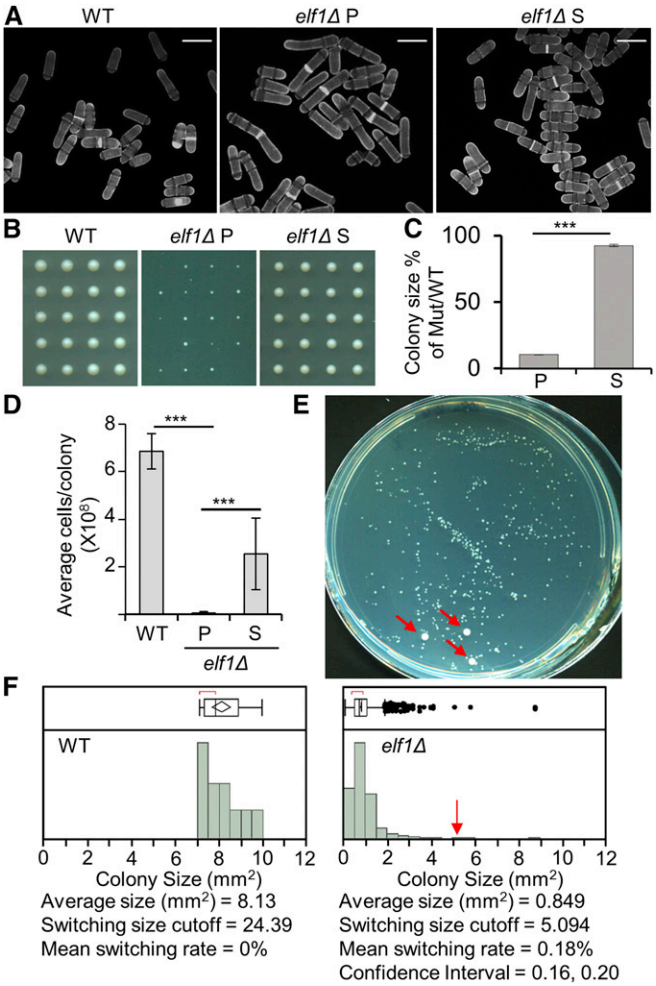

Figure 1 Phenotypic recovery of *elf1Δ* cells. (A) Cell shapes change when *elf1Δ* strains switch from P to S. Cells were observed under a 63× oil magnification lens with calcofluor-white stain. (B) Colony sizes vary significantly between indicated strains. Individual cells were isolated under a dissection microscope and allowed to grow at 30° on rich (YEA) media. All strains were cultured for the exact same amount of time (6 days) and imaged at the same magnification. (C) Average colony sizes for *elf1Δ* strains (P and S) relative to the average colony size of the wild-type control were calculated (n_{wt} = 371, n_p = 2207, n_s = 260), error bars represent SEM. Data were assessed by a Shapiro-Wilk test for normality and a student *t*-test for statistical significance ($P = 3.4 \times 10^{-27}$) using JMP software. (D) Average numbers of cells per colony were counted using a hemocytometer (n_{wt} = 5, n_P = 9, n_S = 19 colonies). * $P \leq 0.05$ as determined by student's *t*-test comparing the indicated strain values with WT values. WT *vs.* P: P = 5.45E−05; P *vs.* S: P = 8.29E−08. (E) *elf1Δ* P cells recover from their slow growth phenotype to a faster-growing strain type, producing larger colonies. All colonies shown were seeded from a single *elf1Δ* P colony. Colonies which have gained the S phenotype are indicated by red arrows. (F) Distribution and boxplot of colony size switching rate. *X*-axis: colony size (square millimeter). Red arrow: the switching size cut off. Boxplot whiskers: minimum and maximum colony sizes without outliers; boxes: interquartile ranges; lines: the medians; diamonds: the means with the 95% confidence intervals (95% CI); red brackets: the shortest halves in which 50% of the observations occur; and dots: outliers. (A–F) All colonies were grown for 6 days at 30° on YEA before imaging and analysis. Individual colony sizes measured with ImageJ.

mutant cells (Day 6). The percentage of mutant cells (Nat^+) present in the mixed culture was used to determine the advantage that the S cells have over P cells in survival competitions (Figure 2D).

Phenotypic recovery frequency calculations

To calculate the frequency of phenotypic recovery, wild-type, *elf1Δ* P, *elf1Δ* P *rnh1Δ*, and *elf1Δ* P *rnh1Δ rnh201Δ* strains were plated, and the size and number of colonies for each strain type was scored. The colony size cutoff ratio of six was used for *elf1Δ* P, *elf1Δ* P *rnh1Δ*, and *elf1Δ* P *rnh1Δ rnh201Δ* strains. Wild-type recovery cutoffs were set as a less conservative cutoff ratio of three, even though no obvious colony size change was observed using this cutoff (Figure 1F and Figure 7). This colony-size cutoff standard was applied for the entire study. Individual colonies of each strain type formed on YEA plates after dissection were directly diluted in water. The cell density was calculated using a hemocytometer, and ~200 cells were plated per YEA plate and spread manually. These plates were grown at 30° for 6 days and then scanned. The sizes of all colonies on the plate were then measured. The number of colonies per plate and the number of colonies that surpassed the 3× (wild-type) or 6× (*elf1Δ*) size threshold were recorded for each plate. The information was also used to calculate the 95% confidence level (95% CI) for phenotypic recovery rates of various strains, which is included in the supporting methods.

RNaseH1 overexpression

RNaseH1 (Rnh1) was placed under a thiamine-repressible *nmt1* promoter (*p3nmt-Rnh1*) (Ohle *et al.* 2016). Overexpression strain phenotypic recovery rates were compared between wild-type, *elf1Δ*, *elf1Δ rnh1Δ*, and *elf1Δ rnh1Δ rnh201Δ* (Figure 7B). All strains were streaked to obtain individual colonies on EMM plates containing thiamine and small colonies were selected. Two independent biological replicates were used for each strain. Individual colonies were diluted to 200–500 cells/ml and plated on EMM (no thiamine, Rnh1 overexpression) to assay for phenotypic recovery rate. Plate imaging and phenotypic recovery rate calculations were performed as described above.

Genomic DNA extraction, library production, and sequencing

A standard protocol was employed for genomic DNA extraction (also see the supporting methods). Genomic libraries were produced for whole-genome sequencing of two *elf1Δ* P strains and five *elf1Δ* S strains using the Illumina TruSeq DNA PCR-Free LT library prep kit. The libraries were prepared following the manufacturer's protocols. The concentrations of the resulting libraries were calculated by running qPCR using KAPA Illumina library quantification kit DNA standards and universal qPCR kit (KK4824). The 16 libraries were combined into two pools and 125 bp paired end sequencing was performed using the Illumina HiSeq2500 platform by the David H. Murdock Research Institute.

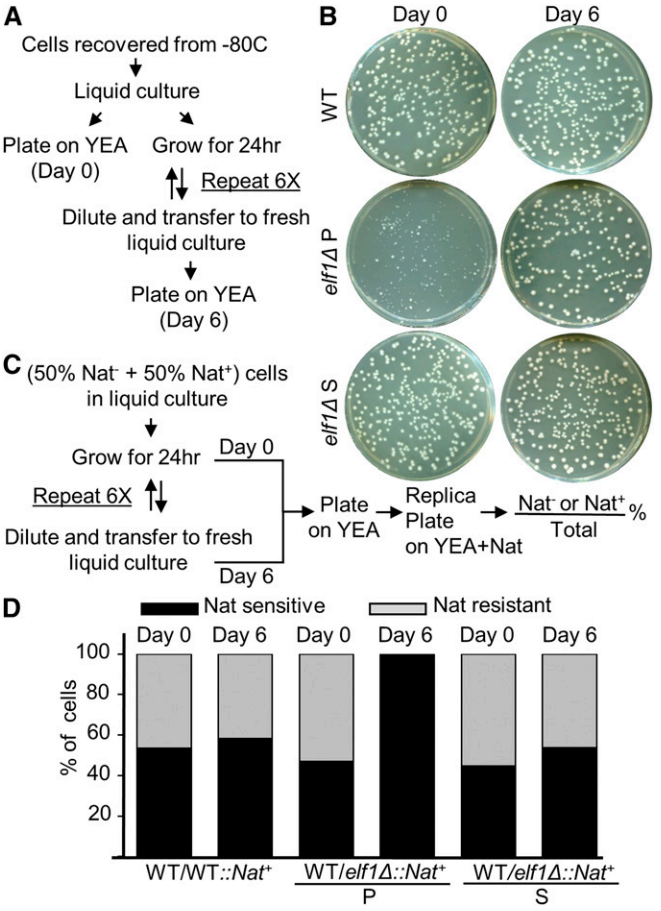

Figure 2 *elf1Δ* S strains have a competitive growth advantage over *elf1Δ* P strains but not wild-type cells. (A and B) P cells are outgrown by S cells. (A) WT, *elf1Δ*P, and *elf1Δ*S cells were grown at 30° in liquid culture with daily transfer and dilution into fresh rich media for 6 days prior to being plated on YEA. (B) Cells were at Day 0 (left column) and the end of Day 6 (right column), then grown for an extra 6 days on YEA plates at 30° before imaging. (C and D) Survival competition assays. (C) A diagram of the experimental design. (D) The profile of the percentage of Nat sensitive (Nat^-) *vs.* resistant (Nat^+) for each mixed culture at the start (0 days) and the end (6 days) of a survival competition assay. The percentage of Nat^+ were determined by dividing the number of colonies growing on YEA containing nourseothricin by the total number of colonies growing on YEA. Both Nat^+ and Nat^- cells make up total 100% of the total number of cells in the mixture.

Short reads were minimally trimmed using SHEAR (https://github.com/jbpease/shear) using the command line (all other options default) provided in the supporting methods. All genomic data are available online at NCBI BioProject PRJNA471808.

DNA-damaging agent stresses

Cells were serially diluted 10-fold and plated on YEA plates with or without 0.05% (5 μg/ml) bleomycin (Figure 5A). The cells growing on YEA plates were exposed to 300 J/m^2 UV using an analytikjena UVP Hybrilinker. After 6 days of growth, the plates were scanned. Wild-type cells were used as a negative control.

Analysis of Rad52-GFP levels

A *rad52*$^{+}$ allele fused to a green fluorescent protein (Rad52-GFP) was incorporated in the genetic background of all strains used. Strains were streaked to individual colonies, and 16 small colonies were picked (small size colonies only applicable in the *elf1Δ*P *rad52-GFP* background). Sixteen individual colonies per strain were suspended in an optical flat-bottom 96-well plate (product number: 353072; BD Falcon) containing 200 μl of rich liquid medium (YEA). Bleomycin (0.05%; 5 μg/ml) was added to 8 out of the 16 individual colonies. Colony growth and GFP signal were measured 1 hr after bleomycin treatment using a microplate reader (Synergy ^{1}H; Biotek Instruments) equipped with monochromator-based optics with an incubation temperature of 30°, and continuous fast orbital shaking. Growth was determined by OD (600 nm) and GFP signal at 395/509 excitation/emission spectra. Readings were recorded every 2 min for 24 hr (total of 720 reads per colony). Bleomycin-treated colonies were normalized to nontreated colonies, and GFP signal reads were normalized to colony growth (OD) read. Curves were generated in Gen5 microplate reader software (Gen5 3.03; Biotek Instruments) as an average of the 8 individual colonies in each of the treatment groups and two biological replicates. Wild-type cells with no Rad52-GFP were included as a negative control.

Cell cycle synchronization by hydroxyurea

For demonstration of cell shape (Figure 1A) and the analysis of lagging chromosomes (Figure 5C), cell cycle synchronization was performed following the standard hydroxyurea (HU) block-release protocol described previously (Luche and Forsburg 2009). Strains were streaked to individual colonies to select for small colonies (small size colonies only applicable in the *elf1Δ* P strains). HU treatment was performed at 30° for 4 hr at 15 mM HU concentration. Cells were subsequently released in EMM media and incubated at 25° for 3 hr, and 1 ml aliquots were taken for subsequent staining and imaging.

Analysis of lagging chromosomes

Identification of chromosome mis-segregation was performed as previously described (Pidoux *et al.* 2000). Cells were imaged using a Zeiss 880 laser scanning confocal microscope with a Zeiss Plan-Apichromat 63x/1.4Oil DIC oil-immersion lens (Figure 5C). Lagging chromosomes were analyzed in 200 late anaphase cells with indicated genotypes of two independent biological replicates. Results are plotted as a calculated percentage of cells with lagging chromosomes to the total number of cells scored (Figure 5D). A two-sample *t*-test was performed by comparing the percentage of cells with lagging chromosomes between *elf1Δ* and the wild-type cells.

Analysis of minichromosome loss

Strains were generated by incorporating a TAS-*ura4*$^{+}$*-tel2* (L) from an artificial minichromosome into wild-type and mutant strains (indicated by +mini in Figure 5, E and F). The endogenous *ura4* locus was truncated in all strains used in this experiment (*ura4DS/E*). All strains containing the minichromosome were confirmed by PCR genotyping, and form single colonies on selective dropout medium lacking uracil (AA-uracil) plates. Single colonies of two independent biological replicates of each genotype were bulked on rich media plates. Strains were plated in relatively uniform rectangular patches on rich media for 24 hr, then replica plated on AA-uracil. Patches were allowed to grow for 7 days, and all plates were scanned to obtain a high-resolution image (Figure 5E). A wild-type strain not containing the minichromosome was used as a negative control (no growth on AA-uracil). Number of colonies in each patch was counted, and results were reported as the average number of individual colonies of each genetic background across biological replicates (Figure 5F). A two-sample *t*-test was performed in *elf1Δ* and wild-type cells.

RNA-fluorescence in situ hybridization

RNA-fluorescence *in situ* hybridization RNA-FISH was carried out as described previously (Reyes-Turcu *et al.* 2011). The images were taken using a Zeiss 880 laser scanning confocal microscope with a Zeiss Plan-Apochromat 63x/1.4Oil DIC oil-immersion lens (Figure 6A). The percentage of cells with RNA accumulation in the nucleus to the total number of cells were scored, and the amount of RNA retention signal was quantified using ImageJ (Figure 6B).

Growth curves generated by microplate reader

Strains with indicated genotypes (Figure 8) were dissected to single cells under a dissecting microscope and grown on YEA plates at 30° for 6 days. Sixteen individual colonies of each strain were suspended in wells containing 200 μl of rich liquid media (YEA) in an optical flat-bottom 96-well plate. Colony growth was measured using a microplate reader with an incubation temperature of 30°, continuous fast orbital shaking, and OD (600 nm) readings every 2 min for 24 hr. Final OD readings were used to redilute each colony down to 0.01 OD in 200 μl of rich medium in a new 96-well plate, which were then grown for another 24 hr with continuous OD reading. This process was repeated for 6 days, with growth curves for individual colonies generated daily and analyzed by Gen5 microplate reader software.

Data availability

The authors affirm that all data necessary for confirming the conclusions of the article are present within the article, figures, and tables. Strains are available upon request. Table S1 contains genotypes for all strains used in this study. Table S2 is a list of all oligonucleotides. Supplemental figures are available in supporting figures and legends file. File S1 contains additional methods section including code used to analyze the genomic data. All genomic data and genomic sequencing raw reads (FASTQ files) are available online at NCBI BioProject PRJNA471808. Supplemental material available at Figshare: https://doi.org/10.25386/genetics.6307136.

Results

Cells lacking Elf1 are growth-deficient and morphologically distinct

Compared to wild-type cells, *elf1Δ* cells show a higher variation in shape and size, with many being abnormally long (Figure 1A). Although cells lacking the Elf1 chromodomain (*elf1CDΔ)* do not have growth defects compared to the wild-type cells (Figure S1), *elf1Δ* cells grow slowly and form abnormally small colonies (Figure 1, B and C). After 6 days of growth, *elf1Δ* colonies occupied an average of 10.4% of the area of wild-type colonies (Figure 1C) because they contain fewer cells (Figure 1D). These results indicate that deletion of *elf1* reduces the growth rate and alters cell size and morphology.

elf1Δ cells have a high rate of spontaneous phenotypic recovery

We observed noticeably high rates of phenotypic recovery in *elf1Δ* strains from slow-growing to faster-growing strain types under standard *S. pombe* culture conditions. These converted strains formed larger colonies that were similar in size to wild-type and significantly larger than those of initial *elf1Δ* strains (Figure 1, A–C and E). Phenotypic recovery occurred at a rate of 0.18% of *elf1Δ* colonies (Figure 1F), while no wild-type colonies were observed to generate spontaneous mutants with such a substantial multi-fold change in size. To distinguish *elf1Δ* cells with different phenotypes, the typical *elf1Δ* parental strains, which form small, slow-growing colonies, were dubbed "P (parental) strains." The suppressed recovery mutant strains with growth rates more similar to wild-type were named "S" (suppressed) strains. We did not observe any reversion from S to P phenotype, suggesting that despite the high rate of phenotypic recovery, *elf1Δ* S cells carry genetic, rather than epigenetic, changes.

elf1Δ S strains have a competitive growth advantage over elf1Δ P but not wild-type cells

To understand the population dynamics of P and S cells in liquid media, we aged cells in liquid cultures for 6 days and analyzed population changes (Figure 2A). We recovered wild-type, *elf1Δ* P, and *elf1Δ* S strains, which were generated from genetic crosses and stored in a −80° freezer. The cells grew into a patch on a YEA plate for 2 days. Since each stored strain was derived from a single cell, the recovered cells of each strain should have the identical genetic background. For each strain, we then transferred a small patch of cells into liquid cultures, and grew them shaking overnight at 30°, and also plated diluted samples on YEA agar plates (Day 0). Each subsequent day, the cultures were diluted to similar prelog phase densities in fresh YEA media and were grown overnight. On the 6th day, samples from each culture were diluted and plated on YEA agar plates (Day 6). After 6 days, the majority of colonies formed by fresh P cells at Day 0 were small and only some of the cells recovered to form bigger healthy colonies (S colonies), but plates seeded with the Day 6 cultures produced only S colonies (Figure 2B). These results indicate that S cells have such a substantial competitive growth advantage over P cells that when an S cell arises in *elf1Δ* P culture, its descendants outcompete those of the P cells.

We next compared the relative fitness of *elf1Δ* P and S strains directly against wild-type (*elf1*$^+$) cells. *elf1*$^+$ (wild-type) cells sensitive to the antibiotic nourseothricin (Nat$^-$) were combined in liquid YEA with an equal amount of nourseothricin-resistant (Nat$^+$) *elf1Δ* mutants (P or S) or *elf1*$^+$ control strains. Samples were plated on YEA immediately after mixing, and again after six daily dilutions in fresh medium followed by overnight growth. Numbers of Nat$^+$ and Nat$^-$ colonies were determined by replica-plating from YEA to YEA+Nat plates, and the frequencies of each competitor were calculated (Figure 2C). The frequencies of Nat$^+$ and Nat$^-$ *elf1*$^+$ strains showed little or no change, indicating that the marker itself had no fitness effect. However, *elf1Δ* P cells were completely absent in mixtures with the *elf1*$^+$ strain (Figure 2D). In contrast, *elf1Δ* S cells showed little or no change in frequencies against the *elf1*$^+$ competitor, indicating that mutation to S effectively restored wild-type fitness.

elf1Δ P to S switching is due to heritable traits

Vegetatively growing *S. pombe* cells are normally haploid. However, when two haploid strains with complementary mating types are subjected to nitrogen starvation, they undergo sexual differentiation and mate. The resulting diploid cell undergoes meiosis, forming a tetrad that contains four haploid daughter spores that show 2:2 segregation of any Mendelian trait in which the parents differed (Figure S2A). The contrasting colony sizes that always segregate from a cross between wild-type and *elf1Δ* P cells (Figure S2, B and C) confirm that P strains do not carry additional mutations other than *elf1Δ* that affect colony size or cell shape. To investigate the inheritance of the phenotypic changes in S strains, we back-crossed *elf1Δ* S cells with wild-type cells, which resulted in a 2:1:1 ratio of wild-type:P:S colony sizes and cell morphologies (Figure S2, D and E). The sizes of colonies formed on fresh plates by cells isolated from P and S colonies remained consistent. Therefore, when *elf1Δ* S strains are backcrossed with wild-type strains, the resulting *elf1Δ* spores consistently form distinct P and S colonies, indicating that S strains contain at least one heritable genetic alteration that suppresses the *elf1Δ* P phenotype and is not tightly linked to *elf1*$^+$.

Phenotypic reversion in different S strains arose by independent mutations

Notably, *elf1Δ* S strains isolated independently from the same P strain grow to sizes significantly different from one another (Figure 3A), prompting us to investigate whether the suppressor mutations in these *elf1Δ* S strains were in the same gene. Strains with complementary mating types were generated for each independently generated S strain, and each was crossed with another S strain that arose separately. If the suppressor mutations in two independently arisen S strains

are located in the same gene, all spores produced by crossing them would show the S phenotype (Figure S2F). In contrast, if the suppressors affected different genes, classic Mendelian genetics would suggest that 25% of the resulting spores would be small and P-like because they only contain *elf1Δ* without a suppressor. In this case, 75% of the spores would receive at least one or two suppressor mutations, causing the resulting colonies to have the S phenotype (Figure S2G). Analysis of 252 tetrads from 23 crosses among independently arisen S strains showed a clear pattern. Only one cross resulted in all medium or all large colonies, indicating mutations in the same gene (Figure S2F). In the remaining crosses between independent *elf1Δ* S strains, 22.3% of the colonies were *elf1Δ* P-like colonies and 77.7% were *elf1Δ* S-like colonies (Figure S2G). We identified five individually isolated S strains (Figure 3A) that do not complement each other, indicating that each of them carries a different suppressor of *elf1Δ*.

Identification of mutations that suppress elf1Δ

Since the phenotypic recovery from P to S cells is due to the presence of additional genetic mutations that suppress the phenotype of *elf1Δ*, we attempted to identify those mutations by sequencing the entire genomes of two *elf1Δ* P strains (triplicates/each) and five individually isolated *elf1Δ* S strains (duplicates/each). Paired-end whole genome sequencing analyses were focused on identification of the genetic differences between the P and the S *elf1Δ* strains. Although we did detect the loss of *elf1*$^+$ and the insertion of an ectopic *ura4*$^+$ allele in the genetic background, we did not observe large sequence deviations between the two types of *elf1Δ* strains, indicating that there were no large genomic duplications or deletions (Figure S3). We identified a total of 660 genomic alterations across all three chromosomes between *elf1Δ* P and the five different S strains (Figure 3B). The majority of the alterations occur in noncoding regions (Figure 3C). Although 75% of the nucleotide changes are insertion mutations (INDEL, Figure 3D), we did not observe identical mutations between sequenced biological replicates of each strain, suggesting that either new mutations may arise during the culture of *elf1Δ* cells before genomic library construction or random errors may be introduced during the library construction. When focused on the genomic changes that are consistently identified between P and S *elf1Δ* strains in biological replicates, we found that only seven genomic changes are located within coding regions (Figure 3E), but four of them are synonymous (Figure 3F). The genes with nonsynonymous point mutations or INDELs in both sequencing replicates of an S strain include *cue2*$^+$, *rpl2702*$^+$, and *SPBPJ4664.02*$^+$ (*Gsf2-like*) (Figure 3G). The *cue2* mutant (*cue2-1*) is missing amino acids 396–400 (R-S-L-A-M), and the 45th amino acid of *rpl2702* is changed from glycine to aspartate (G45D). By conducting genetic crosses, we were able to verify that *cue2-1* cosegregated with *elf1Δ* S cells but not with P cells (Figure 4A). In addition, deletion of *cue2*$^+$ (*cue2Δ*) rescues the *elf1Δ* P phenotype (Figure 4B),

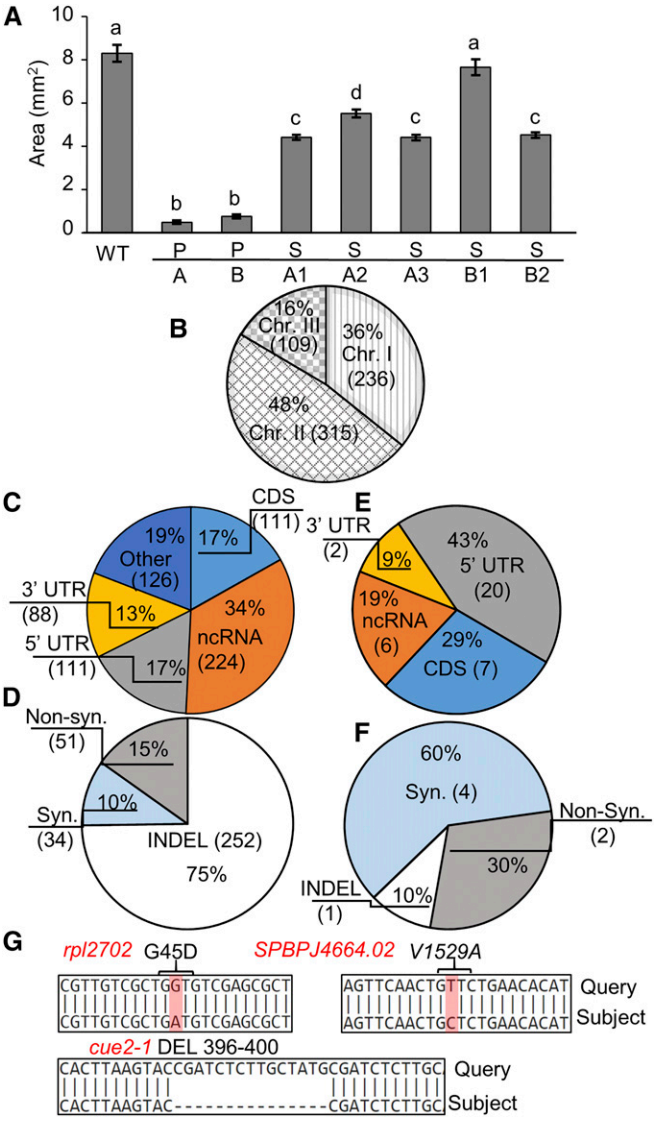

Figure 3 Genomic sequencing identifies suppressors of *elf1Δ*. (A) Most independently arisen *elf1Δ* S strains show different colony sizes. Average sizes of colonies of individual strains with indicated genotypes. "A" and "B" refer to two independently generated parental strains (P), numbers refer to individually arisen switched strains (S) derived from "A" or "B." The B1 strain contains *cue2-1* in addition to *elf1Δ*. Error bars represent SEM (n_{wt} = 20, n_{PA} = 15, n_{PB} = 12, n_{SA1} = 20, n_{SA2} = 19, n_{SA3} = 20, n_{SB1} = 20, and n_{SB2} = 19). Statistical significance was calculated using a one-way ANOVA test (F = 129.1, P = 1.9 × 10^{-16}). Multiple pairwise comparisons were performed, and different alphabetical letters denote significant difference based on a *post hoc* Tukey test run in SPSS. (B–D) Pie-charts represent sequence variations between suppressor strains and their respective parental strains across all five suppressor strains sequenced, classified by (B) chromosome number; (C) genomic region; (D) type of mutation. (E and F) Pie-charts represent selected sequence variations that meet the requirement of being consistent between biological replicates of suppressor strains as compared to their respective parental strains. (E) genomic region, (F) type of mutations for selected sequence variations that fall within the coding sequence, and are consistent across biological replicates of suppressor strains, (G) exact sequence variation found in the genes in (F).

indicating that the *cue2* mutation is indeed a suppressor of *elf1Δ* P cells. The same genetic analysis also confirmed that *rpl2702* mutants (*rpl2702G45D* or *rpl2702Δ*) suppress the loss of *elf1Δ* (Figure 4, C and D). *SPBPJ4664.02*$^{+}$ is a large gene (11,916 nt), and contains highly repetitive elements surrounding the putative mutation sites, which complicate the verification of the mutations using conventional DNA sequencing. However, the whole genomic sequencing data suggests that these mutations are nonsynonymous point mutations. Although we have not been able to verify whether this mutant would cosegregate with the *elf1Δ* S phenotype, it is likely that this *gsf2-like* mutation also acts as a suppressor of *elf1Δ* P. Loss of either *cue2* or *rpl2702* causes mild growth defects (Figure 4) because they form colonies slightly smaller than the wild-type cells. Since *cue2-1* is the strongest confirmed suppressor of *elf1Δ*, we will focus on this suppressor for the rest of the study.

Loss of function of Cue2 reverses the genome instability caused by elf1Δ

The fast phenotypic recovery of *elf1Δ* P cells suggests that cells lacking Elf1 are susceptible to genomic instability. We analyzed the growth behavior and DNA-damage sensitivity of *elf1Δ* cells using *clr6* mutants as a positive control. Clr6 is the class I histone deacetylase (HDAC) in fission yeast, well known for its important role in maintaining genome stability (Nicolas *et al.* 2007). Bleomycins, used clinically as chemotherapy drugs, are a group of natural glycopeptides that induce sequence-specific single DNA breaks and DSBs through a free radical-based mechanism (Chen *et al.* 2008). DNA damage can also be induced by ultraviolet (UV) light (Houtgraaf *et al.* 2006). We found that *elf1Δ* P strains showed sensitivity to bleomycin and UV radiation (Figure 5A), suggesting that either double-strand DNA-repair is compromised, or that the additional stress of DSBs on top of loss of *elf1*$^{+}$ may lead to cell death. Notably, *cue2-1 elf1Δ* double mutant cells are not sensitive to bleomycin compared to wild-type cells, suggesting that loss of function of Cue2 compensates the susceptibility of *elf1Δ* cells to DNA damage.

To further investigate whether more DNA damage occurs in *elf1Δ* P cells in response to genotoxic stress, we compared the levels of Rad52-GFP between wild-type and *elf1Δ* in the presence of bleomycin. Rad52 is an essential protein for DNA DSB repair and homologous recombination (Mortensen *et al.* 1996; Lok and Powell 2012). We observed significantly enhanced levels of Rad52-GFP in *elf1Δ* P cells than that of wild-type cells after bleomycin treatment, indicating that the DNA damage response is prominent in *elf1Δ* P cells (Figure 5B). As expected, once combined with *cue2Δ*, *elf1Δ* P cells did not exhibit noticeably enhanced Rad52-GFP in response to DNA damage, consistent with the suppression of *elf1Δ* by *cue2Δ* in DNA damage response and repair (Figure 5B).

The additional evidence for the genome instability of *elf1Δ* P cells was collected by monitoring the frequencies of lagging chromosomes on late anaphase spindles, using DAPI to stain DNA (Pidoux *et al.* 2000). Counting only late anaphase cells

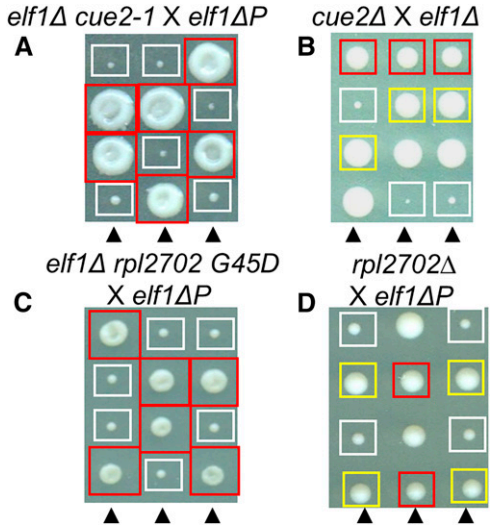

Figure 4 The confirmation of *cue2* and *rpl2702* mutations as suppressors of *elf1Δ*. Tetrads resulting from the mating of (A) a *cue2-1 elf1Δ* strain with an *elf1Δ* P strain, (B) a *cue2Δ* strain with an *elf1Δ* P strain, (C) an *elf1Δ rpl2702 G45D* and an *elf1Δ* P strain, and (D) *rpl2702 Δ* with an *elf1Δ* P strain. (A–D) Vertical tetrads correspond to colonies grown from the each of the four haploid spores of mated haploid parental strains, indicated by triangles. No box, wild-type; white boxes, *elf1Δ* colonies; red boxes, (A) *elf1Δ cue2-1*, (B) *elf1Δ cue2Δ*, (C) *elf1Δ rpl2702 G45D* or (D) *elf1Δ rpl2702 Δ*; and yellow boxes, (B) *cue2Δ* colonies or (D) *rpl2702 Δ*.

(spindle >10 μm), we found that chromosomes mis-segregated significantly more often in *elf1Δ* cells (11%) compared to wild-type (1%) or *elf1Δ cue2-1Δ* (1.75%) cells (Figure 5, C and D). We also tested chromosomal instability in wild-type and mutant cells by monitoring the frequency of chromosome loss using a nonessential mini-chromosome (Niwa *et al.* 1989) (Figure 5, E and F). Replica-plating from YEA medium to uracil dropout medium demonstrated the ability of maintaining the mini-chromosome in various yeast strains because only cells retaining the mini-chromosome will grow on the uracil dropout medium. *elf1Δ* and *clr6-1* cells demonstrated higher rates of losing the mini-chromosome compared to the wild-type and the *cue2Δ elf1Δ* double mutant cells (Figure 5, E and F). These results support that the loss of function of Cue2 suppresses the genome instability in *elf1Δ* P cells.

cue2 mutants suppress RNA nuclear retention in elf1Δ P cells

Elf1 was implicated in mRNA export, although mRNA accumulation was not observed in *elf1Δ* cells by RNA-FISH (Kozak *et al.* 2002). To rule out the possibility that the RNA-FISH conducted in the previous study may have used *elf1Δ* S cells, we revisited the function of Elf1 in RNA nuclear export by conducting RNA-FISH using a Cy3-labled oligo-dT probe (Figure 6). As a control, we included cells with the deletion of *rrp6*, the nuclear-specific exosome subunit, which causes accumulation of RNAs within the nucleus upon loss

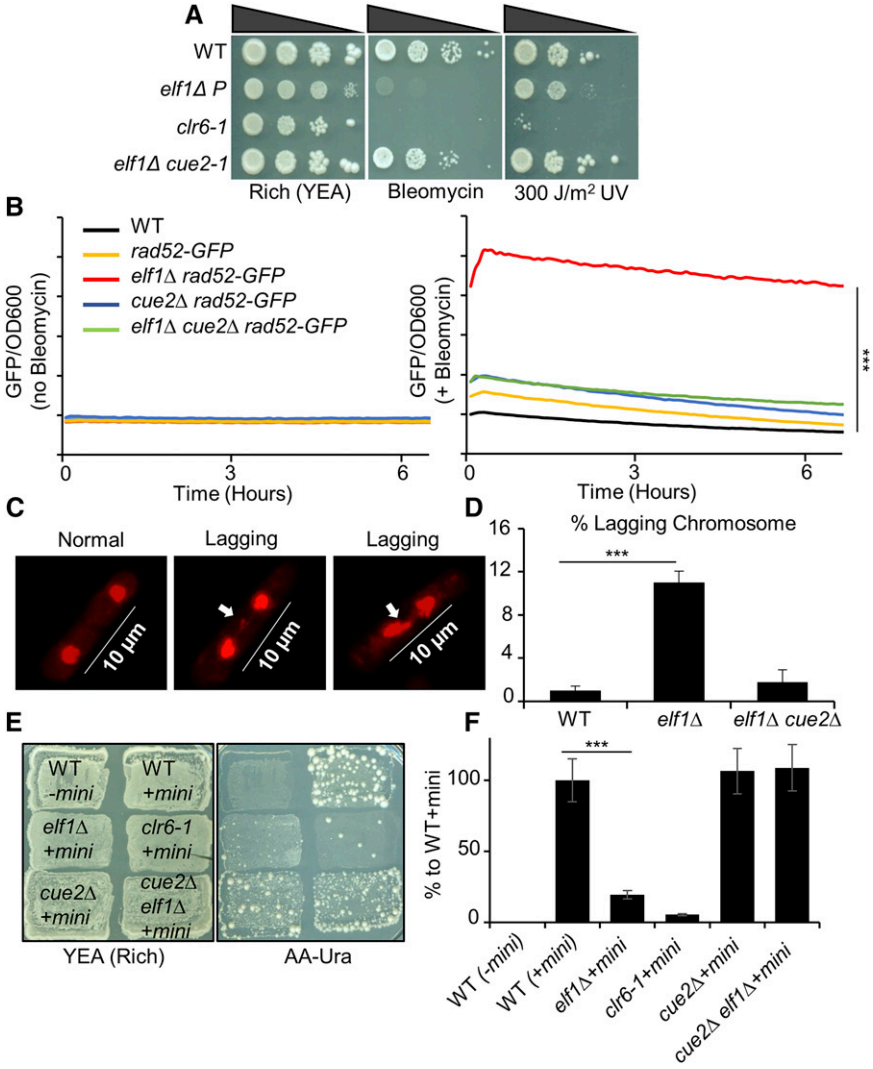

Figure 5 *cue2Δ* alleviates genomic instability in *elf1Δ* strains. (A) *cue2-1* suppresses the sensitivity to DNA damaging agents of *elf1Δ*. Serial dilution assay of strains with indicated genotypes. (B) Rad52-GFP plate-reader fluorescence detection assay. Strains were grown in YEA with or without Bleomycin as indicated on the *Y*-axis. Signal reported as GFP fluorescence over total culture growth ($OD_{595\ nm}$). Asterisks denote significant difference comparing *elf1Δ* to *elf1Δ cue2Δ* ($P = 3.78 \times 10^{-5}$). (C) Examples of one normal and two lagging chromosomes in HU-synchronized cells as observed with confocal microscopy. Bar indicates 10 μm. (D) Quantification of the lagging chromosome experiment. The *Y*-axis is the percentage of dividing cells with lagging chromosomes *vs.* the total number of late anaphase cells counted per strain. Asterisks denote a significant difference in the percent of lagging chromosomes in *elf1Δ vs.* that of wild-type strains ($P = 0.00049$). (E) Sample plates of the minichromosome loss experiment. (F) Quantification of the minichromosome loss rate (%) was calculated by dividing the number of colonies growing on AA-uracil for each strain by the number of colonies counted on the wild-type (with minichromsome) strain. Asterisks denote significant differences comparing the minichromosome loss rate between wild-type and *elf1Δ* strains ($P = 0.0016$).

of function. In wild-type cells, RNAs were uniformly distributed in the cell and do not show obvious accumulation within the nucleus. As expected, ~67.5% of *rrp6Δ* cells accumulated RNA within the nucleus. We also observed nuclear RNA accumulation in 14.5% of *elf1Δ* P cells (Figure 6A). Although average detected oligo-dT-Cy3 signals were stronger in *rrp6Δ* compared to *elf1Δ* cells ($P = 7.6 \times 10^{-8}$), the detected signal in *elf1*Δ cells is significantly higher than the wild-type cells, indicating nuclear RNA retention. We did not see any RNA accumulation in *elf1Δ cue2-1* cells, indicating that *cue2-1* also suppresses *elf1Δ*-associated nuclear RNA accumulation. The low percentage of *elf1Δ* P cells that show obvious RNA nuclear retention is likely caused by the recovering of the P cells to S cells during the culture preparation of RNA FISH. Altogether, our results indicate that *cue2-1* rescues the growth defect, the sensitivity to DNA-damaging agents, chromosome instability, and the RNA export defect of *elf1Δ*, suggesting that Cue2 and Elf1 work in the same pathway in RNA metabolism, and that their functions are essential in preventing genome instability.

Modulating RNase H activities in elf1Δ P cells affects rates of phenotypic recovery

Given that RNA can mediate mutagenesis (Keskin *et al.* 2014), the build-up of RNAs in the nucleus of *elf1Δ* cells might contribute to the genome instability via increased formation of R-loops or increased misincorporation of ribonucleotides into DNA. These DNA–RNA hybrids are known to interfere with transcription, protein binding, and the assembly of nucleosomes (Aguilera and García-Muse 2012; Williams *et al.* 2016), and are endogenously resolved by RNase H (Rydberg and Game 2002; Gavaldá *et al.* 2013). Without RNase H, cells cannot efficiently break down mutagenic DNA–RNA hybrid structures. We tested whether the accumulation of DNA–RNA hybrids contributes to the generation of *elf1Δ* suppressor mutations. If so, the enhanced accumulation of DNA–RNA hybrids caused by the loss of RNase H enzymes would further increase the phenotypic recovery rates of *elf1Δ* P cells. When the two RNase H genes (*rnh1*$^+$ and *rnh201*$^+$) in *S. pombe* were deleted in *elf1Δ* P cells, the frequency of suppressor generation in rich medium increased greater than fourfold

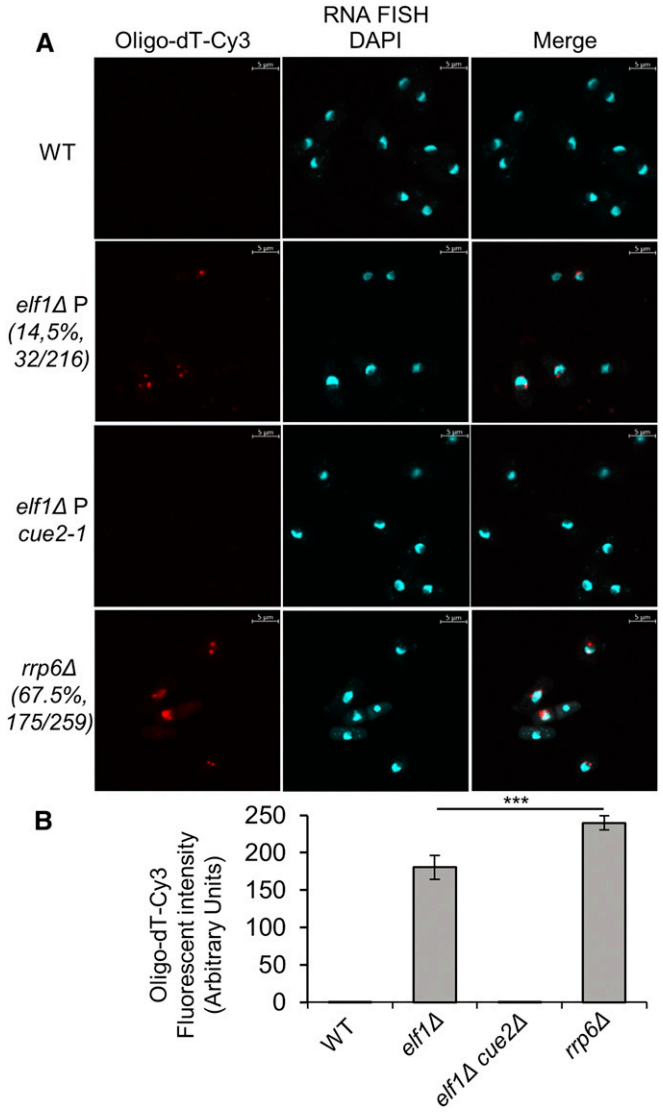

Figure 6 *elf1Δ* P cells accumulate RNAs in the nucleus. (A) RNA export defects (nuclear retention of RNA) of indicated strains are examined by RNA-FISH. Probe: oligo-dT-Cy3. (B) Amount of RNA retention signal was quantified using ImageJ. Accumulated RNA signals in scored cells were graphed ($n_{elf1\Delta}$ = 30, $n_{rrp6\Delta}$ = 22). Scale bar: 5μM. Error bars represent the 95% CI.

from 0.18 to 0.85% (Figure 7A). Considering the loss of RNase H is known to increase the rate of mutation (Nick McElhinny *et al.* 2010), we also overexpressed RNase H1 in *elf1Δ* P cells and analyzed the resulting phenotypic recovery rate. Notably, overexpression of *nmt-rnh1*$^+$ on minimal medium (EMM no thiamine) resulted in a significant decrease in phenotypic recovery rates in the *elf1Δ* cells. Surprisingly, the phenotypic recovery rates of *elf1Δ*, *elf1Δ rnh1Δ*, and *elf1Δ rnh1Δ rnh201Δ* strains were all increased when we cultured the cells on EMM medium compared to YEA medium (Figure 7, cf. panels B and A), suggesting that the stress of caloric restriction may enhance the phenotypic recovery in *elf1Δ* cells. Nevertheless, the significant decrease in phenotypic recovery rates of *elf1Δ* P to S cells when Rnh1 is overexpressed suggests that the nuclear RNA retention of *elf1Δ* may increase the formation of DNA–RNA hybrids that contribute to the enhanced phenotypic recovery rates and genome instability.

Nuclear RNA retention is correlated with rapid phenotypic recovery

Defects in several nuclear processes, such as RNA export and nuclear RNA degradation, cause nuclear RNA retention. In *S. pombe*, loss of either RNA export factor Mlo3 (an ortholog of the budding yeast YRA1) or nuclear-specific exosome subunit Rrp6 also causes nuclear RNA retention and defective growth (Reyes-Turcu *et al.* 2011; Paul and Montpetit 2016), similar to *elf1Δ*. To compare the dynamic changes of growth rates in liquid culture for wild-type, *elf1Δ*, *mlo3Δ*, and *rrp6Δ* strains, we isolated individual cells using a dissection microscope, allowed them to form colonies, and traced the growth curves of 16 colonies per strain over 6 days in liquid culture (Figure 8). At Day 0, all of the *elf1Δ* P colonies exhibited growth curves that lag behind wild-type and *elf1Δ cue2-1* strains due to their growth defect. However, by Day 6, 25% of *elf1Δ* P colonies had clearly converted to S cells and displayed growth curves similar to those observed in wild-type or *elf1Δ cue2-1*. Expectedly, *clr6-1*, a well-known mutation that causes genome instability (Nicolas *et al.* 2007), also demonstrated quick phenotypic recovery, indicating the gain of suppressor mutations. Notably, although both *mlo3Δ and rrp6Δ* cells show improved growth rates by Day 6, they do not recover to the near-wild-type growth rates observed in *elf1Δ* P and *clr6-1* cells, suggesting that the functions of these proteins can only be partially compensated by suppressors. It seems that all mutants that exhibit growth defects and accumulate RNA within nucleus can recover their fitness after growing in liquid culture for 6 days, indicating that long-term liquid culture is a powerful way of screening for suppressor mutations.

Discussion

In this study, we detail a mechanism by which *elf1Δ* overcomes its own immediate effects on growth rate, likely related to the accumulation of DNA–RNA hybrids and acquisition of suppressor mutations (Figure S4).

An auto-suppression phenotype without Elf1

When we first generated an *elf1Δ* strain, we observed a severe growth defect (Figure 1, A–C). Unexpectedly, when we recovered the stored *elf1Δ* strain from an ultra-low temperature freezer, we found no obvious growth defect in *elf1Δ* cells compared to the wild-type cells. This phenotypic difference was caused by the fact that *elf1Δ* cells can recover from the slow-growing, small colony-forming P cell phenotype to the wild-type-like S cell phenotype. The recovery occurs without additional environmental interference; *elf1Δ* P cells are capable of "fixing" their own growth defects. Our later genetic analyses indicated that our original P cells converted to S cells before storage, with all converted strains carrying compensatory mutations. This self-suppression phenotype has

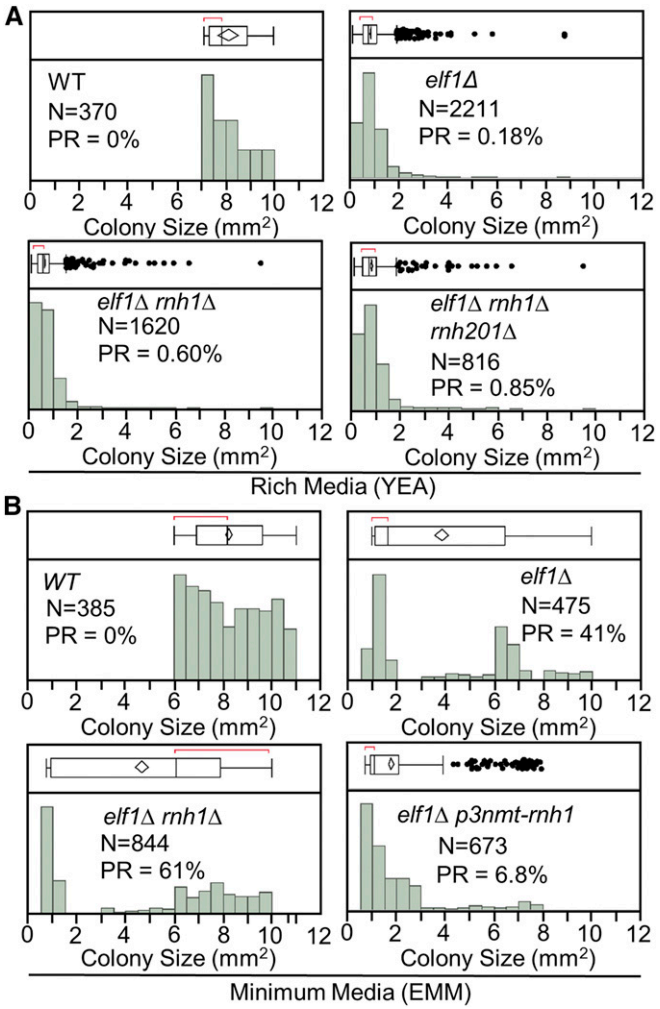

Figure 7 The phenotypic recovery rate of *elf1Δ* is increased by mutations in RNase H and decreased by overexpression of RNase H1. (A) Strains with mutated RNase H show an increase in phenotypic recovery rate (PR). Distribution and boxplots of colony areas when strains are grown on YEA media. (B) Colony size pattern shows a recovery rate decrease in the Rnh1 overexpression strain. (A and B) Mean recovery rates and confidence intervals were calculated. Boxplot whiskers: minimum and maximum colony sizes without outliers, boxes: interquartile ranges, lines: the medians, diamonds: the means with the 95% CI, red brackets: the shortest halves in which 50% of the observations occur, and dots: outliers, but not necessarily those that pass the recovery rate cutoff as calculated (B).

been previously reported in other studies using fission yeast as a model organism. For example, several studies failed to identify the essential role of Rad22 (Rad52 ortholog) due to the presence of suppressor mutations in the *rad22* mutant background (Osman *et al.* 2005). Laboratory manipulation of microorganisms and cell lines inevitably use liquid culture, a process that is selective for fitness because faster-growing cells will become dominant in the population over time.

To ensure that we examined the veritable phenotype in fission yeast caused by loss of Elf1, we isolated individual cells using a dissection microscope, and analyzed the phenotypes of the resulting colonies. We observed slow growth phenotypes that affected both cell shape and colony size in *elf1Δ* P strains. Similarly, loss of the Elf1 ortholog in *Candida albicans* causes distinctly slow growth, forming misshapen, aggregated cells (Sturtevant *et al.* 1998; Kozak *et al.* 2002). Another phenotypic-screen study in *S. pombe* found that *elf1Δ* cells had a distinctly long morphology, and places Elf1 in a group of proteins involved in mRNA metabolism and interphase progression (Hayles *et al.* 2013). While not specifically investigated in the study of *C. albicans*, Sturtevant *et al.* (1998) did notice that the misshapen cells were outgrown by the more "normally shaped" cells. This likely correlates to what we observed with S cells overgrowing P cells when aging liquid population cultures of *elf1Δ* P cells for several days (Figure 2, A and B). When stored cells were growing in liquid cultures diluted daily, *elf1Δ* S cells arose in cultures of *elf1Δ* P cells and eventually overtook the entire culture, becoming the only cell type recovered after 6 days. Also, when *elf1Δ* cells were in direct competition for survival with wild-type cells, P cells were readily outgrown by wild-type cells, but S cells were not (Figure 2, C and D).

elf1Δ P to S recovery is attributed to genetic traits rather than an epigenetic mechanism

When P cells are grown on plates for 6 days, <15 generations of cells are generated because of the slow rate of cell division (~10 hr/generation). However, we observed that 0.18% of P colonies switched to faster-growing S cells (Figure 1F). Usually, the cause of such a quick change of phenotype can be explained by epigenetic instead of genetic phenomena. If the phenotypic recovery from P to S is caused by changing the chromatin structure within the nucleus, then this recovery should be reversible. However, once recovered, S cells do not revert back to P cells under the same growth conditions, suggesting that it is unlikely that an epigenetic mechanism causes this "self-suppression." In addition, we considered the formation of prions in the cytoplasm of S cells as another potential epigenetic mechanism mediating this recovery. Prions were especially intriguing when looking into the role of Elf1 in *S. pombe* because the ortholog of Elf1 in *S. cerevisiae* is NEW1, which promotes the formation and breakdown of other prions, and can even form a prion itself (Inoue *et al.* 2011; Du and Li 2014). However, while there is sequence similarity between these orthologs, Elf1 in *S. pombe* lacks the putative N-terminal prion-forming domain that NEW1 contains, making it much less likely to form a prion. We attempted to detect the presence of a prion in S cells by "curing" them using guanidinium chloride, which prevents propagation of prions causing dilution and even complete loss of the prion in newer generations of the population (Eaglestone *et al.* 2000). This method was unable to prevent recovering from P to S *elf1Δ* cells, and did not "cure" existing S *elf1Δ* cells, suggesting that it is not prion formation in S cells that suppresses P phenotype.

Our genetic analyses clearly indicate that the phenotypic recovery from *elf1Δ* P to S cells is due to the acquisition of suppressor mutations. Although we uncovered five complementation groups, suggesting that five different suppressors

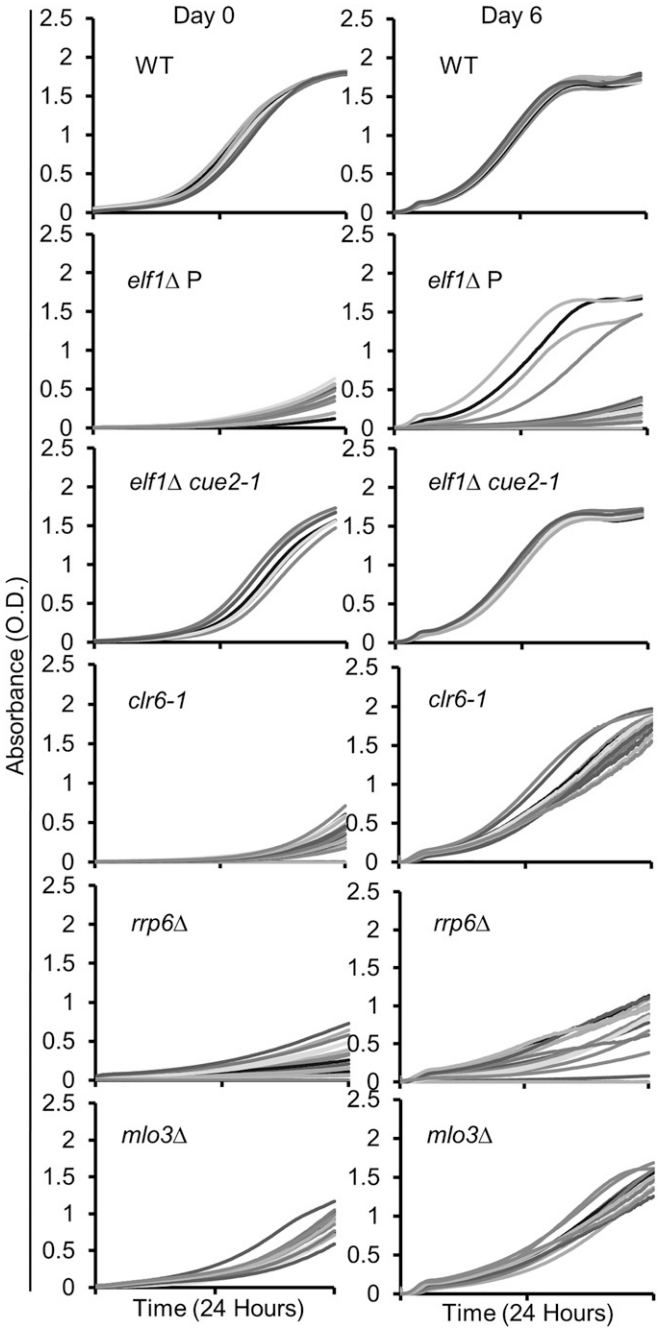

Figure 8 *elf1Δ* P cells demonstrate a unique growth recovery pattern in liquid culture. Growth curves of 16 individual colonies of each indicated strain were generated daily for 6 days of continuous growing with daily dilutions. *X*-axis: time (24 hr); *Y*-axis: $OD_{595\ nm}$.

should be identified in our whole genome DNA sequencing, we identified only three mutations occurring in gene coding regions that suppress *elf1Δ*, including *cue2*$^+$, *rpl2702*$^+$, and *SPBPJ4664.02*$^+$. The other two mutations were identified in noncoding regions, and whether they can suppress *elf1Δ* will be explored in our future studies. These three genes have not been functionally linked and their relation to, and potential regulation of, one another is intriguing. Curiously, when Farlow *et al.* (2015) investigated *S. pombe*'s spontaneous mutation rate, they identified changes in flocculation-related genes in 20 out of 96 total cell lines measured, a significantly higher rate of mutation than was observed in any other type of gene. The gene that they detected the most mutations in was a gene that we identified as a suppressor, *SPBPJ4664.02*$^+$. The effect of environmental stressors on *S. pombe* cells can be mitigated by flocculation, which suggests that the genes that regulate flocculation harbor a large number of the mutations because their alteration may protect the cell (Farlow *et al.* 2015). Conversely, they may simply be more prone to mutation themselves and have an abnormally high mutation rate (Farlow *et al.* 2015). In addition, the average length of exons of *S. pombe* genes is <1011 nucleotides, but *SPBPJ4664.02*$^+$ is a very long gene, containing 12,260 nucleotides with no introns. The long length of the gene provides >11 times as much area to be modified compared to the average gene, potentially skewing results.

Cue2 and Rpl2702 have not been functionally characterized previously. We chose to focus on Cue2 in this study because *cue2-1* has the strongest effect in suppressing the susceptibility to DNA damage and nuclear RNA retention caused by the loss of Elf1 (Figure 4, Figure 5, and Figure 6). The budding yeast homolog of Cue2 contains two ubiquitin-binding CUE motifs (Kang *et al.* 2003), and the human homolog, NEDD4-binding protein 2 like 2 (N4BP2L2), may contribute to neutropenia through mediating the cooperation of transcriptional repression between GFI1 and neutrophil elastase (Salipante *et al.* 2009). The CUE motif suggests a role of Cue2 in facilitating intramolecular monoubiquitination (Shih *et al.* 2003). In addition to the CUE motif, Cue2 has an SMR domain, which implies a function in mismatch repair (Fukui and Kuramitsu 2011). Despite the domain information, the biological functions of Cue2 are almost completely unknown. *cue2-1* may suppress *elf1Δ* through (1) resuming RNA export, (2) enhancing the degradation of nuclear RNAs, (3) promoting DNA damage repair, and/or (4) preventing the formation of abnormal DNA–RNA hybrids caused by nuclear RNA retention. Detailed characterization of this functional connection in our future study will uncover novel mechanistic functions of Elf1 and Cue2.

Increased rate of phenotypic switching of elf1Δ mutants without RNase H activities

Since Elf1 plays a role in mRNA transport, the likely proximal cause of the mutations and the source of the genomic instability could be tied to the accumulation of mRNA within the nucleus (Kozak *et al.* 2002). We found that a distinct increase in the amount of RNA was observed in the nucleus of *elf1Δ* P cells in comparison to wild-type cells (Figure 6). The coupled transcription, messenger ribonucleoprotein (mRNP) biogenesis, and export processes prevent accumulation of newly produced mRNA within the nucleus. Impairment of these processes may cause nascent RNA retention at the transcribed loci and promote R-loop accumulation (Bhatia *et al.* 2017). With a large number of R-loops accumulating, they may not be resolved promptly, exposing many sections of

DNA to potential breaks (Bhatia *et al.* 2017). In addition, the functional connection between Elf1 and Cue2, which may involve mismatch repair, suggests that misincorporation of ribonucleotides into DNA could be another potential mechanism to mediate the self-suppression phenotype. Nevertheless, RNase H activities are required to remove either R-loops or misincorporated ribonucleotides (Rydberg and Game 2002; Aguilera and García-Muse 2012). The dramatic changes in the phenotypic recovery rate between wild-type cells, *elf1Δ* P cells, *elf1Δ rnh1Δ rnh201Δ* P cells, and *elf1Δ* cells overexpressing Rnh1, suggest the intriguing possibility that the buildup of RNA, likely resulting in enhanced R-loop formation or misincorporated ribonucleotides, contributes to the source of the genomic instability in *elf1Δ* cells.

A unique self-suppression pattern in elf1Δ cells

Growth curves generated by a microplate reader allow us to dynamically follow the phenotypic recovery of different mutations with growth defects over time (Figure 8). Even though liquid culture is selective for fitness, after continuously growing for 6 days, all 16 wild-type colonies display tightly overlapped growth curves, indicating the limitation of the ability to improve the fitness of the wild-type cells. All mutants with growth defects improved their growth rates after 6 days of selection for fitness, acquiring suppressor mutations. Thus, if a mutant has growth defect, a long-term liquid culture of the mutant cells with daily dilution in fresh medium can be used as a powerful method for suppressor screening. Intriguingly, mutants such as *elf1Δ* and *clr6-1*, quickly recovered growth rates near to that of wild-type cells, indicating that their functions can be replaced by mutation of other genes. Although cells without Elf1, Mlo3, or Rrp6 share a common feature: accumulation of RNAs in the nucleus, their growth curves exhibit different phenotypic recovery patterns (Figure 8), indicating that nuclear RNA retention is correlated with, but may not be sufficient to induce, the self-suppression phenotype. Loss of *rrp6*, for example, cannot be fully compensated by suppressors, indicating the unreplaceable function of this nuclear exoribonuclease. An Elf1-specific, RNase activity-related mechanism mediates the quick phenotypic recovery observed in *elf1Δ* cells. Once made, nuclear RNAs are quickly exported, sequestered within nuclear structures such as the nucleolus, or degraded. Our study highlights the essential function of RNA export in preventing genome instability by avoiding the accumulation of RNAs within the nucleus.

Acknowledgments

We thank Shiv Grewal and Tamás Fischer for sharing strains. We thank Glen Marrs and Heather Brown-Harding for help with confocal image acquisition. We also thank Hugh Cam, Gloria Muday, and Sarah McDonald for comments on the manuscript. Miaohua Jiang suggested formula for calculating the size switching rate. This work is supported by the National Institute of General Medical Sciences, grants 1R15GM119105-01 to K.Z.

Literature Cited

Aguilera, A., and T. García-Muse, 2012 R loops: from transcription byproducts to threats to genome stability. Mol. Cell 46: 115–124. https://doi.org/10.1016/j.molcel.2012.04.009

Aguilera, A., and T. García-Muse, 2013 Causes of genome instability. Annu. Rev. Genet. 47: 1–32. https://doi.org/10.1146/annurev-genet-111212-133232

Al-Sady, B., H. D. Madhani, and G. J. Narlikar, 2013 Division of labor between the chromodomains of HP1 and Suv39 methylase enables coordination of heterochromatin spread. Mol. Cell 51: 80–91. https://doi.org/10.1016/j.molcel.2013.06.013

Bähler, J., J. Q. Wu, M. S. Longtine, N. G. Shah, A. McKenzie, III *et al.*, 1998 Heterologous modules for efficient and versatile PCR-based gene targeting in Schizosaccharomyces pombe. Yeast 14: 943–951. https://doi.org/10.1002/(SICI)1097-0061(199807)14:10<943::AID-YEA292>3.0.CO;2-Y

Bhatia, V., E. Herrera-Moyano, A. Aguilera, and B. Gomez-Gonzalez, 2017 The role of replication-associated repair factors on R-loops. Genes (Basel) 8: 171. https://doi.org/10.3390/genes8070171

Cerritelli, S. M., and R. J. Crouch, 2009 Ribonuclease H: the enzymes in eukaryotes. FEBS J. 276: 1494–1505. https://doi.org/10.1111/j.1742-4658.2009.06908.x

Chen, J., M. K. Ghorai, G. Kenney, and J. Stubbe, 2008 Mechanistic studies on bleomycin-mediated DNA damage: multiple binding modes can result in double-stranded DNA cleavage. Nucleic Acids Res. 36: 3781–3790. https://doi.org/10.1093/nar/gkn302

Ciccia, A., and S. J. Elledge, 2010 The DNA damage response: making it safe to play with knives. Mol. Cell 40: 179–204. https://doi.org/10.1016/j.molcel.2010.09.019

Costantino, L., and D. Koshland, 2015 The Yin and Yang of R-loop biology. Curr. Opin. Cell Biol. 34: 39–45. https://doi.org/10.1016/j.ceb.2015.04.008

Dowell, R. D., O. Ryan, A. Jansen, D. Cheung, S. Agarwala *et al.*, 2010 Genotype to phenotype: a complex problem. Science 328: 469. https://doi.org/10.1126/science.1189015

Drolet, M., P. Phoenix, R. Menzel, E. Masse, L. F. Liu *et al.*, 1995 Overexpression of RNase H partially complements the growth defect of an Escherichia coli delta topA mutant: R-loop formation is a major problem in the absence of DNA topoisomerase I. Proc. Natl. Acad. Sci. USA 92: 3526–3530. https://doi.org/10.1073/pnas.92.8.3526

Du, Z., and L. Li, 2014 Investigating the interactions of yeast prions: [SWI+], [PSI+], and [PIN+]. Genetics 197: 685–700. https://doi.org/10.1534/genetics.114.163402

Eaglestone, S. S., L. W. Ruddock, B. S. Cox, and M. F. Tuite, 2000 Guanidine hydrochloride blocks a critical step in the propagation of the prion-like determinant [PSI(+)] of Saccharomyces cerevisiae. Proc. Natl. Acad. Sci. USA 97: 240–244. https://doi.org/10.1073/pnas.97.1.240

Farlow, A., H. Long, S. Arnoux, W. Sung, T. G. Doak *et al.*, 2015 The spontaneous mutation rate in the fission yeast Schizosaccharomyces pombe. Genetics 201: 737–744. https://doi.org/10.1534/genetics.115.177329

Forsburg, S. L., 2001 The art and design of genetic screens: yeast. Nat. Rev. Genet. 2: 659–668. https://doi.org/10.1038/35088500

Forsburg, S. L., 2003 Growth and manipulation of S. pombe. *Curr. Protoc. Mol. Biol.* Chapter 13: Unit 13.16. https://doi.org/10.1002/0471142727.mb1316s64

Fukui, K., and S. Kuramitsu, 2011 Structure and function of the small MutS-related domain. Mol. Biol. Int. 2011: 691735. https://doi.org/10.4061/2011/691735

Gaillard, H., E. Herrera-Moyano, and A. Aguilera, 2013 Transcription-associated genome instability. Chem. Rev. 113: 8638–8661. https://doi.org/10.1021/cr400017y

Gavaldá, S., M. Gallardo, R. Luna, and A. Aguilera, 2013 R-loop mediated transcription-associated recombination in trf4Δ mutants reveals new links between RNA surveillance and genome integrity. PLoS One 8: e65541. https://doi.org/10.1371/journal.pone.0065541

Harper, A. R., S. Nayee, and E. J. Topol, 2015 Protective alleles and modifier variants in human health and disease. Nat. Rev. Genet. 16: 689–701. https://doi.org/10.1038/nrg4017

Hayles, J., V. Wood, L. Jeffery, K. L. Hoe, D. U. Kim *et al.*, 2013 A genome-wide resource of cell cycle and cell shape genes of fission yeast. Open Biol. 3: 130053. https://doi.org/10.1098/rsob.130053

Hou, J., A. Friedrich, J. S. Gounot, and J. Schacherer, 2015 Comprehensive survey of condition-specific reproductive isolation reveals genetic incompatibility in yeast. Nat. Commun. 6: 7214. https://doi.org/10.1038/ncomms8214

Houtgraaf, J. H., J. Versmissen, and W. J. van der Giessen, 2006 A concise review of DNA damage checkpoints and repair in mammalian cells. Cardiovasc. Revasc. Med. 7: 165–172. https://doi.org/10.1016/j.carrev.2006.02.002

Inoue, Y., S. Kawai-Noma, A. Koike-Takeshita, H. Taguchi, and M. Yoshida, 2011 Yeast prion protein New1 can break Sup35 amyloid fibrils into fragments in an ATP-dependent manner. Genes Cells 16: 545–556. https://doi.org/10.1111/j.1365-2443.2011.01510.x

Jorgensen, E. M., and S. E. Mango, 2002 The art and design of genetic screens: Caenorhabditis elegans. Nat. Rev. Genet. 3: 356–369. https://doi.org/10.1038/nrg794

Kang, R. S., C. M. Daniels, S. A. Francis, S. C. Shih, W. J. Salerno *et al.*, 2003 Solution structure of a CUE-ubiquitin complex reveals a conserved mode of ubiquitin binding. Cell 113: 621–630. https://doi.org/10.1016/S0092-8674(03)00362-3

Keskin, H., Y. Shen, F. Huang, M. Patel, T. Yang *et al.*, 2014 Transcript-RNA-templated DNA recombination and repair. Nature 515: 436–439. https://doi.org/10.1038/nature13682

Kozak, L., G. Gopal, J. H. Yoon, Z. E. Sauna, S. V. Ambudkar *et al.*, 2002 Elf1p, a member of the ABC class of ATPases, functions as a mRNA export factor in Schizosaccharomyces pombe. J. Biol. Chem. 277: 33580–33589. https://doi.org/10.1074/jbc.M205415200

Lesnik, E. A., and S. M. Freier, 1995 Relative thermodynamic stability of DNA, RNA, and DNA:RNA hybrid duplexes: relationship with base composition and structure. Biochemistry 34: 10807–10815. https://doi.org/10.1021/bi00034a013

Lok, B. H., and S. N. Powell, 2012 Molecular pathways: understanding the role of Rad52 in homologous recombination for therapeutic advancement. Clin. Cancer Res. 18: 6400–6406. https://doi.org/10.1158/1078-0432.CCR-11-3150

Luche, D. D., and S. L. Forsburg, 2009 Cell-cycle synchrony for analysis of S. pombe DNA replication. Methods Mol. Biol. 521: 437–448. https://doi.org/10.1007/978-1-60327-815-7_24

Manson, M. D., 2000 Allele-specific suppression as a tool to study protein-protein interactions in bacteria. Methods 20: 18–34. https://doi.org/10.1006/meth.1999.0902

Mortensen, U. H., C. Bendixen, I. Sunjevaric, and R. Rothstein, 1996 DNA strand annealing is promoted by the yeast Rad52 protein. Proc. Natl. Acad. Sci. USA 93: 10729–10734. https://doi.org/10.1073/pnas.93.20.10729

Nakayama, J., A. J. Klar, and S. I. Grewal, 2000 A chromodomain protein, Swi6, performs imprinting functions in fission yeast during mitosis and meiosis. Cell 101: 307–317. https://doi.org/10.1016/S0092-8674(00)80840-5

Nakayama, J., J. C. Rice, B. D. Strahl, C. D. Allis, and S. I. Grewal, 2001 Role of histone H3 lysine 9 methylation in epigenetic control of heterochromatin assembly. Science 292: 110–113. https://doi.org/10.1126/science.1060118

Nick McElhinny, S. A., D. Kumar, A. B. Clark, D. L. Watt, B. E. Watts *et al.*, 2010 Genome instability due to ribonucleotide incorporation into DNA. Nat. Chem. Biol. 6: 774–781. https://doi.org/10.1038/nchembio.424

Nicolas, E., T. Yamada, H. P. Cam, P. C. Fitzgerald, R. Kobayashi *et al.*, 2007 Distinct roles of HDAC complexes in promoter silencing, antisense suppression and DNA damage protection. Nat. Struct. Mol. Biol. 14: 372–380. https://doi.org/10.1038/nsmb1239

Niwa, O., T. Matsumoto, Y. Chikashige, and M. Yanagida, 1989 Characterization of Schizosaccharomyces pombe minichromosome deletion derivatives and a functional allocation of their centromere. EMBO J. 8: 3045–3052.

Ohle, C., R. Tesorero, G. Schermann, N. Dobrev, I. Sinning *et al.*, 2016 Transient RNA-DNA hybrids are required for efficient double-strand break repair. Cell 167: 1001–1013.e7. https://doi.org/10.1016/j.cell.2016.10.001

Osman, F., J. Dixon, A. R. Barr, and M. C. Whitby, 2005 The F-Box DNA helicase Fbh1 prevents Rhp51-dependent recombination without mediator proteins. Mol. Cell. Biol. 25: 8084–8096. https://doi.org/10.1128/MCB.25.18.8084-8096.2005

Paul, B., and B. Montpetit, 2016 Altered RNA processing and export lead to retention of mRNAs near transcription sites and nuclear pore complexes or within the nucleolus. Mol. Biol. Cell 27: 2742–2756. https://doi.org/10.1091/mbc.e16-04-0244

Pidoux, A. L., S. Uzawa, P. E. Perry, W. Z. Cande, and R. C. Allshire, 2000 Live analysis of lagging chromosomes during anaphase and their effect on spindle elongation rate in fission yeast. J. Cell Sci. 113: 4177–4191.

Pleasance, E. D., R. K. Cheetham, P. J. Stephens, D. J. McBride, S. J. Humphray *et al.*, 2010 A comprehensive catalogue of somatic mutations from a human cancer genome. Nature 463: 191–196. https://doi.org/10.1038/nature08658

Reyes-Turcu, F. E., K. Zhang, M. Zofall, E. Chen, and S. I. Grewal, 2011 Defects in RNA quality control factors reveal RNAi-independent nucleation of heterochromatin. Nat. Struct. Mol. Biol. 18: 1132–1138. https://doi.org/10.1038/nsmb.2122

Rydberg, B., and J. Game, 2002 Excision of misincorporated ribonucleotides in DNA by RNase H (type 2) and FEN-1 in cell-free extracts. Proc. Natl. Acad. Sci. USA 99: 16654–16659. https://doi.org/10.1073/pnas.262591699

Salipante, S. J., M. E. Rojas, B. Korkmaz, Z. Duan, J. Wechsler *et al.*, 2009 Contributions to neutropenia from PFAAP5 (N4BP2L2), a novel protein mediating transcriptional repressor cooperation between Gfi1 and neutrophil elastase. Mol. Cell. Biol. 29: 4394–4405. https://doi.org/10.1128/MCB.00596-09

Shih, S. C., G. Prag, S. A. Francis, M. A. Sutanto, J. H. Hurley *et al.*, 2003 A ubiquitin-binding motif required for intramolecular monoubiquitylation, the CUE domain. EMBO J. 22: 1273–1281. https://doi.org/10.1093/emboj/cdg140

Shim, Y. S., Y. Choi, K. Kang, K. Cho, S. Oh *et al.*, 2012 Hrp3 controls nucleosome positioning to suppress non-coding transcription in eu- and heterochromatin. EMBO J. 31: 4375–4387. https://doi.org/10.1038/emboj.2012.267

Skourti-Stathaki, K., and N. J. Proudfoot, 2014 A double-edged sword: R loops as threats to genome integrity and powerful regulators of gene expression. Genes Dev. 28: 1384–1396. https://doi.org/10.1101/gad.242990.114

Sollier, J., and K. A. Cimprich, 2015 Breaking bad: R-loops and genome integrity. Trends Cell Biol. 25: 514–522. https://doi.org/10.1016/j.tcb.2015.05.003

St Johnston, D., 2002 The art and design of genetic screens: Drosophila melanogaster. Nat. Rev. Genet. 3: 176–188. https://doi.org/10.1038/nrg751

Stratton, M. R., P. J. Campbell, and P. A. Futreal, 2009 The cancer genome. Nature 458: 719–724. https://doi.org/10.1038/nature07943

Sturtevant, J., R. Cihlar, and R. Calderone, 1998 Disruption studies of a Candida albicans gene, ELF1: a member of the

ATP-binding cassette family. Microbiology 144: 2311–2321. https://doi.org/10.1099/00221287-144-8-2311

Taylor, M. B., J. Phan, J. T. Lee, M. McCadden, and I. M. Ehrenreich, 2016 Diverse genetic architectures lead to the same cryptic phenotype in a yeast cross. Nat. Commun. 7: 11669. https://doi.org/10.1038/ncomms11669

Touat-Todeschini, L., E. Hiriart, and A. Verdel, 2012 Nucleosome positioning and transcription: fission yeast CHD remodellers make their move. EMBO J. 31: 4371–4372. https://doi.org/10.1038/emboj.2012.284

Williams, J. S., S. A. Lujan, and T. A. Kunkel, 2016 Processing ribonucleotides incorporated during eukaryotic DNA replication. Nat. Rev. Mol. Cell Biol. 17: 350–363. https://doi.org/10.1038/nrm.2016.37

Zhang, K., K. Mosch, W. Fischle, and S. I. Grewal, 2008 Roles of the Clr4 methyltransferase complex in nucleation, spreading and maintenance of heterochromatin. Nat. Struct. Mol. Biol. 15: 381–388. https://doi.org/10.1038/nsmb.1406

Communicating editor: J. Nickoloff